Synthesis of MCM-41 stabilized NZVI and its use in removal of Cr(VI) from aqueous solution

Mang Lu, Yue Cheng, Jian-min Pan, Wen-jing Fan, Chuang Jiao and Xiao-yu Liu

ABSTRACT

In this study, MCM-41 stabilized nano zero-valent iron (M-NZVI) is synthesized using the rheological phase reaction method. Characterization with transmission electron microscopy validates the hypothesis that the introduction of MCM-41 leads to a decrease in aggregation of iron nanoparticles. X-ray diffraction confirms the existence of Fe^0 and the strong antioxidant activity of Fe^0 nanoparticles. Batch Cr(VI) reduction experiments exhibit that solution pH, M-NZVI dosage, and reaction time have significant effects on Cr(VI) removal. A high removal efficiency of Cr(VI) (84.5%) is obtained within 60 min for 100 mg/L of Cr(VI) solution at an initial pH of 6.0 and M-NZVI dosage of 0.5 g/L at 35 °C. The Cr(VI) removal rates follow modified pseudo-first-order kinetic equations. The observed removal rate constant was 0.0168/min for the M-NZVI dosage of 1.0 g/L. Our study suggests that the introduction of an innocuous stabilizer such as MCM-41 can significantly improve the performance of Fe^0 nanoparticles for environmental remediation applications.

Key words | kinetics, nano zero-valent iron, rheological phase reaction method, zeolite

Mang Lu
Yue Cheng (corresponding author)
Wen-jing Fan
Chuang Jiao
Xiao-yu Liu
School of Materials Science and Engineering,
Jingdezhen Ceramic Institute,
Jingdezhen 333403,
Jiangxi,
China
E-mail: *cy_jci@163.com*

Jian-min Pan
School of Chemistry and Chemical Engineering,
Shanghai University of Engineering Science,
Shanghai 201620,
China

INTRODUCTION

Chromium compounds are widely applied in a variety of industrial processes such as textile dying, steel, ferro- and nonferrous alloys, refractories, pigments, electroplating, tanning, and others (Kotaś & Stasicka 2000). Thereupon, accidental leakage, unsuitable storage, and/or improper disposal practices often result in the release of chromium to the environment (Alidokht *et al.* 2011).

In the natural environment, chromium often exists in two highly stable oxidation states, namely trivalent, Cr(III), and hexavalent, Cr(VI). Cr(III) has a low solubility ($<10^{-5}$ M) and low toxicity, being considered an essential nutrient for many organisms (Kotaś & Stasicka 2000). In contrast, Cr(VI) is up to 1,000-fold more toxic than Cr(III), and it has been added to the Class A Human Carcinogens list by the US Environmental Protection Agency (US EPA) (Richard & Bourg 1991). Therefore, Cr(VI) must be removed from wastewater before discharge to the environment.

Several methods are available for removing Cr(VI) from contaminated wastewater, including membrane separation (Güell *et al.* 2008), chemical reduction (Jagupilla *et al.* 2009; Chrysochoou *et al.* 2010), electrokinetic remediation (Zhang *et al.* 2010), bioremediation (Masood & Malik 2011), and phytoremediation (Zazo *et al.* 2008), to mention a few. Among these methods, chemical reduction followed by precipitation has been considered the most common technique for removing Cr(VI) from wastewater (Alidokht *et al.* 2011).

In recent years, many researchers have demonstrated that nano zero-valent iron (NZVI) can serve as an effective reducing agent for *in situ* reductive removal of Cr(VI) (Wu *et al.* 2009; Wang *et al.* 2010; Alidokht *et al.* 2011; Fang *et al.* 2011; Li *et al.* 2012; Nahuel Montesinos *et al.* 2014; Wang *et al.* 2014). To prevent aggregation and facilitate the transport of NZVI in field conditions, NZVI has been modified with several kinds of organic and inorganic coatings,

doi: 10.2166/wrd.2014.081

such as starch (Alidokht *et al.* 2011), Fe_3O_4 (Wu *et al.* 2009), bentonite (Li *et al.* 2012), and carboxymethyl cellulose (Wang *et al.* 2010; Wang *et al.* 2014). However, these kinds of iron-based materials prepared with traditional methodologies consume a lot of chemical reagents such as ferrous sulfate and ferrous chloride, which result in high production costs and limit further engineering applications. However, these kinds of NZVI particles were synthesized using traditional methodologies, which involve an inert reduction atmosphere and a series of more or less complicated technologies, resulting in high production costs and limitation in practical engineering application.

The rheological phase reaction method is a process for preparing compounds or materials from a solid–liquid rheological mixture, which has many advantages such as efficient utilization of surface area of solid particles, close and uniform contact between solid particle and fluid, good heat exchange, and good control of reaction temperature (Cong *et al.* 2005; Kima *et al.* 2011).

Mesoporous zeolite MCM-41 has received extensive research interest due to high porosity, large specific surface area (up to 1,000 m^2/g or higher), and narrow pore size distribution. MCM-41 has been proved very useful as an adsorbent, a catalyst/support, and a nano-reactor for various materials synthesis due to its excellent properties (Yang *et al.* 2014).

The objectives of this study were: (1) to synthesize MCM-41 stabilized NZVI (M-NZVI) by using the rheological phase reaction method; (2) to study the effects of different parameters (such as nanoparticle dosage, solution pH, and reaction time) on Cr(VI) reduction in aqueous solution by M-NZVI; (3) to investigate the kinetics model fitting with Cr(VI) removal by M-NZVI nanocomposites; and (4) to explore the possible mechanism for the reduction of Cr(VI) by M-NZVI.

MATERIALS AND METHODS

Synthesis of MCM-41

MCM-41 was prepared by a direct hydrothermal synthesis method using cationic surfactant cetyltrimethylammonium bromide (CTAB) as a template and silica sol (25%, $\rho = 0.15\ g/cm^3$) as silicon source under basic conditions. Typically, 2.184 g of CTAB was dissolved into a solution containing 54 mL of deionized water and 0.48 g of NaOH, 10.43 mL of silica sol was then added dropwise under continuous stirring. The final molar composition of the gel was $SiO_2/CTAB/NaOH/H_2O = 1{:}0.12{:}0.24{:}70$. The mixture was stirred at 50 °C for another 2 h, and then aged at 50 °C overnight. Afterwards, the gel was transferred to a Teflon-lined autoclave and crystallized at 85 °C for 48 h. After cooling to room temperature, the crystalline solid was taken out of the autoclave and filtered, repeatedly washed with deionized water until the filtrate was neutral, and then dried at 80 °C for 2 h. To remove the organic template, the samples were annealed at 550 °C in air for 6 h, and then cooled in a desiccator to constant weight.

Preparation of MCM-41 stabilized NZVI

M-NZVI particles were prepared in water by reducing Fe(II) to Fe(0) using KBH_4 in the presence of MCM-41 as a stabilizer. M-NZVI was prepared based on the final mass ratio of MCM-41/NZVI = 1:1, 2:1, or 4:1. Typically, for 4:1 ratio sample, 4.96 g $FeSO_4{\cdot}7H_2O$ was dissolved in a mixture of 30 mL ethanol and 20 mL deionized water. Then 4 g MCM-41 was added to this solution and the mixture was stirred with a magnetic stirrer for 2 h and then oscillated by ultrasound for 0.5 h. Afterwards, under continuous stirring, 50 mL of 1.0 M KBH_4 solution was added dropwise to the Fe(II)/MCM-41/water/ethanol mixture to obtain a rheological body. The mixture was stirred for another 10 min. The final molar ratio of the mixture was $BH^{4-}/Fe^{2+} = 3{:}1$. All the reactions were conducted under continuous stirring at room temperature under the continuous purge of nitrogen gas. The resultant M-NZVI particles were collected by magnetic separation, washed with deionized water and ethanol three times, and finally dried at 60 °C under vacuum.

Characterization of materials

X-ray diffraction (XRD) patterns were obtained from a Bruker D8 advance diffractometer (Bruker, Germany) with Cu Kα radiation from 5 to 70° at a rate of 0.2°/s. The tube current was 100 mA with a tube voltage of 40 kV. The micromorphology was characterized by transmission electron

microscope (TEM) on a high-resolution transmission electron microscope (HR-TEM, JEOL JEM-2010, Japan) with an acceleration voltage of 200 kV.

Batch Cr(VI) removal experiments

The Cr(VI) reduction experiments were carried out in batch conditions at 35 °C and atmospheric pressure in stoppered 250 mL Erlenmeyer flasks, containing 100 mL of Cr(VI) solution on a temperature-controlled shaker with continuous stirring at 250 rpm. Single-factor test was used for investigating the effects of reaction time, initial concentration of Cr(VI), initial solution pH, and dosage of M-NZVI particles on Cr(VI) removal efficiency. The initial solution pH was adjusted with 0.1 M HCl or 0.1 M NaOH solution.

To investigate the role that MCM-41 and Fe^0 played in the M-NZVI system, MCM-41 and NZVI were also used independently in batch experiments examining Cr(VI) removal from aqueous solution (pH 6.0) at an initial concentration of 100 mg/L at 35 °C and 250 rpm. As the optimum mass ratio of MCM-41/Fe^0 was 4:1 in the M-NZVI system, the dosages of MCM-41 and NZVI were set at 0.4 and 0.1 g/L, respectively.

After a desired time, the solutions were filtered using a 0.22 μm cellulose membrane filter to separate the solid particles and solution. The supernatant was then analyzed for Cr(VI) using the 1,5-diphenylcarbazide method with a 722 UV–Vis spectrophotometer (Shanghai Precision & Scientific Instrument Co. Ltd, China), operated at 540 nm wavelength (Geng *et al.* 2009). The data obtained from the batch experiments were then used to calculate the removal efficiency of Cr(VI) by Equation (1):

$$E_{\text{removal}} = \frac{(C_0 - C_t)}{C_0} \times 100\% \quad (1)$$

where C_0 and C_t are the concentrations of Cr(VI) in solution at time $t = 0$ and $t = t$, respectively.

Kinetics of Cr(VI) removal

The kinetic process of Cr(VI) removal was studied in stoppered 250 mL Erlenmeyer flasks, containing 100 mL of 100 mg/L Cr(VI) solution and 0.1 g M-NZVI. The initial solution pH was 6. The kinetics of Cr(VI) reduction was determined at 7-min interval (0–42 min). In this study, all reduction experiments were performed in triplicate to get reliable data, and results represent the average of three parallel experiments.

RESULTS AND DISCUSSION

XRD analysis

XRD patterns of freshly synthesized MCM-41 and M-NZVI particles are presented in Figure 1.

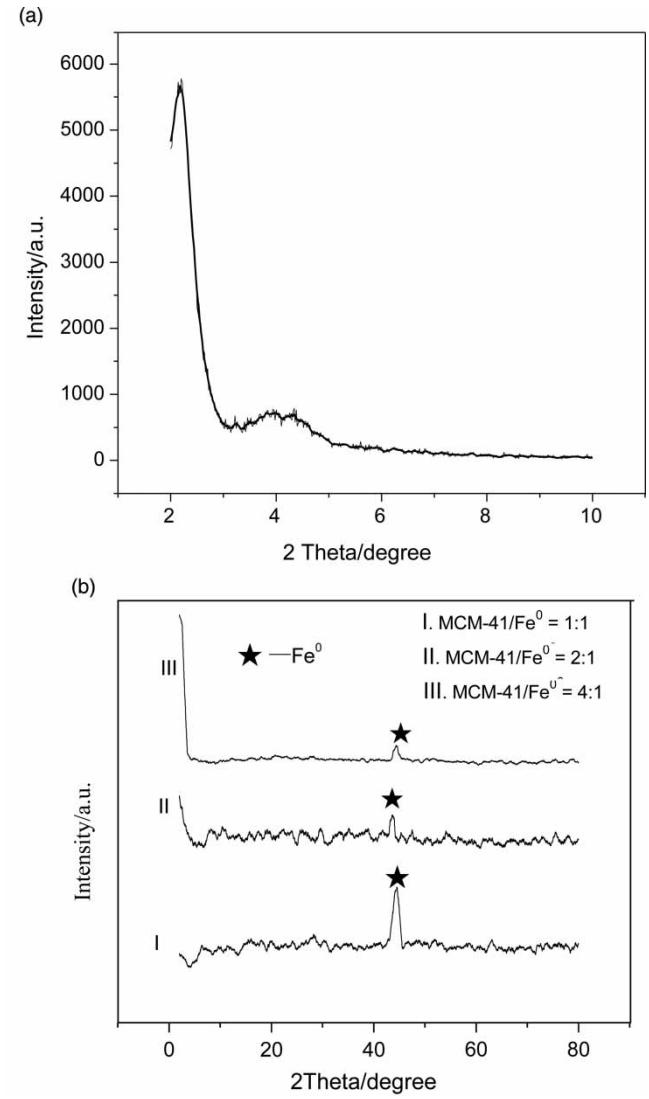

Figure 1 | XRD patterns of (a) laboratory synthesized MCM-41 and (b) M-NZVI samples.

As shown in Figure 1(a), the product has a distinct broad peak at $2\theta = 2.1–2.5^{\circ}$, which is typical of the hexagonal structure of MCM-41 material (Kresge *et al.* 1992). In addition, the sample exhibits several small diffraction peaks at $2\theta = 3–6^{\circ}$, which can be indexed on a hexagonal lattice as (100), (110), (200), and (210). The 2θ position of the diffraction angle of the (100) plane is varied, indicating different interplanar spacings among the (100) plane of the MCM-41 sample.

Figure 1(b) shows the powder XRD patterns of a series of M-NZVI with varied Fe^0 content. A characteristic diffraction peak at 44.7° 2θ degrees indicates the crystallization of Fe^0 nanoparticles. In the low 2θ region of 1–10°, three diffraction peaks indexed as (100), (110), and (200) lattice planes can be observed, which are the characteristic peaks of hexagonal MCM-41 mesoporous material. However, it can be clearly observed that the intensity of these peaks becomes lower with the increase of the iron content. This may be due to the excess of iron destroying the mesoporous structure of MCM-41. Moreover, in the high 2θ region of 10–80°, all of the three types of M-NZVI with varied Fe^0 content exhibit the presence of body-centered cubic α-Fe (110) ($2\theta = 44.83^{\circ}$) and no signal for iron oxides ($2\theta = 35.46^{\circ}$, 43.12°, 53.50°, 56.98°, and 62.64°) is observed. This demonstrates that the prepared M-NZVI has a strong antioxidant activity. Thus, M-NZVI particles with a (MCM-41):Fe^0 mass ratio of 4:1 were used in the subsequent batch Cr(VI) removal experiments.

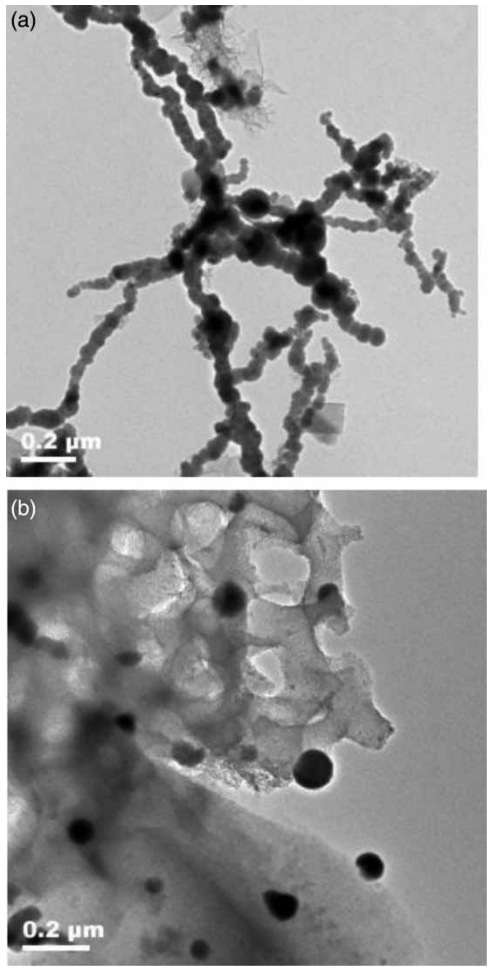

Figure 2 | TEM images of laboratory synthesized (a) NZVI and (b) M-NZVI. The M-NZVI particles have a (MCM-41):Fe^0 mass ratio of 4:1.

TEM analysis

Figure 2(a) shows TEM images of the synthesized nanoscale Fe^0. NZVI has a smooth surface, and a spherical shape for single particle with diameters of 20–50 nm. The spherical nanoparticles aggregate to form larger dendritic structures, due to the geomagnetic forces between nanoscale particles and small particles as well as their surface tension interactions (Wu *et al.* 2009).

The TEM image of the MCM-41 stabilized NZVI particles as shown in Figure 2(b). It can be observed that NZVI particles are encapsulated into the microspheres by a thin layer of mesoporous structure and are isolated from each other. No aggregation of NZVI particles is observed. In addition, lattice fringes can be observed on the surface of the thin layer, indicating the MCM-41 sample possesses high crystallinity. Round-shaped pores with mean diameter of 3–5 nm distributed regularly on the aggregate surface can be observed in Figure 2(b). These results also demonstrate that the mechanical alloying results in a significant dispersion of NZVI and the covering of the MCM-41 surface with very small NZVI particles.

Effect of reaction time

As shown in Figure 3, at a given experimental condition, Cr(VI) removal by M-NZVI and bare NZVI proceeds rapidly within the first 30 min, and then slows down and reaches equilibrium at 60 min with a removal efficiency of 84.5% and 72.3%, respectively. This indicates that the

dominant mechanism for Cr(VI) removal is most likely due to the adsorption to the surface of Fe^0 nanoparticles and then reduction rather than the direct reduction transformation in the aqueous phase (Geng *et al.* 2009; Wang *et al.* 2010). The removal efficiency of Cr(VI) is only 4.6% for MCM-41 after 60 min, indicating the low adsorption of Cr(VI) by the zeolite.

In aqueous solution, NZVI particles will react with water to generate Fe(II), which will then react with Cr(VI) rapidly, resulting in the disappearance of Cr(VI) from the aqueous phase in the second stage (Wang *et al.* 2010). It has been demonstrated that the dissolution of ferrous ions and electrons to react with Cr(VI) by NZVI in the aqueous phase is a fairly fast process (Wu *et al.* 2009). During the early stages of the reaction, Cr(VI) ions can be easily transported to the Fe^0 surface because of the strong adsorption and reduction ability of NZVI. As the reaction continues, the surface reactivity sites of NZVI particles are gradually taken over by corrosion products including iron oxides layers (Fe_3O_4, Fe_2O_3, $Fe(OH)_3$, and FeOOH) (Mielczarski *et al.* 2005) and Fe(III)–Cr(III) hydroxides (Alowitz & Scherer 2002). The formation of this surface passivation layer on NZVI particles will accordingly block Cr(VI) reduction. Figure 3 also shows that bare NZVI particles have a lower reactivity than M-NZVI particles, which may be due to aggregation of bare NZVI particles in aqueous solution. M-NZVI particles apparently do not aggregate as much, as demonstrated in Figure 2(b), yielding a greatly enhanced removal efficiency. Compared with other investigations related to Cr(VI) reduction by NZVI (Wu *et al.* 2009; Wang *et al.* 2010; Alidokht *et al.* 2011; Fang *et al.* 2011; Li *et al.* 2012; Nahuel Montesinos *et al.* 2014; Wang *et al.* 2014), the results of the present study are in good agreement.

Effect of solution pH

As shown in Figure 4, the Cr(VI) removal efficiency increases significantly with decreasing pH. The final Cr(VI) removal by M-NZVI declines from 94.0 to 64.9% when the initial pH increases from 2.0 to 12.0. This indicates that the reduction of Cr(VI) by NZVI is strongly pH-dependent. At low pH, iron is readily soluble and oxide films will not be formed immediately after the start of the experiment, leading to increment in the reduction rate of Cr(VI) (Wu *et al.* 2009). In addition, the increase in H^+ concentration left the surface of MCM-41 less negatively charged, which will reduce the electrostatic repulsion between MCM-41 and Cr(VI) anions. But the increase in pH value will promote the formation of mixed iron oxides and Fe(III)–Cr(III) hydroxides on the iron surfaces, resulting in a decrease in the reaction rate and extent (Wu *et al.* 2009).

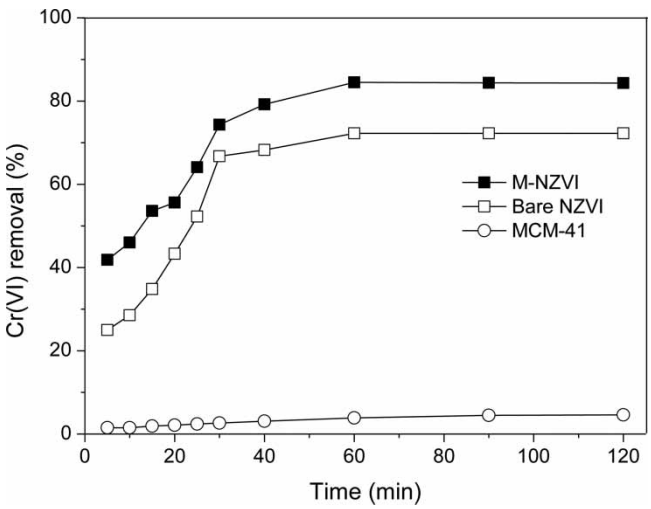

Figure 3 | Effect of reaction time on Cr(VI) removal by MCM-41, bare NZVI, and M-NZVI. The M-NZVI particles have a (MCM-41):Fe^0 mass ratio of 4:1. $[Cr(VI)]_0 = 100$ mg/L, $[M\text{-}NZVI]_0 = 0.5$ g/L, $[MCM\text{-}41]_0 = 0.4$ g/L, $[NZVI]_0 = 0.1$ g/L, and $[pH]_0 = 6.0$.

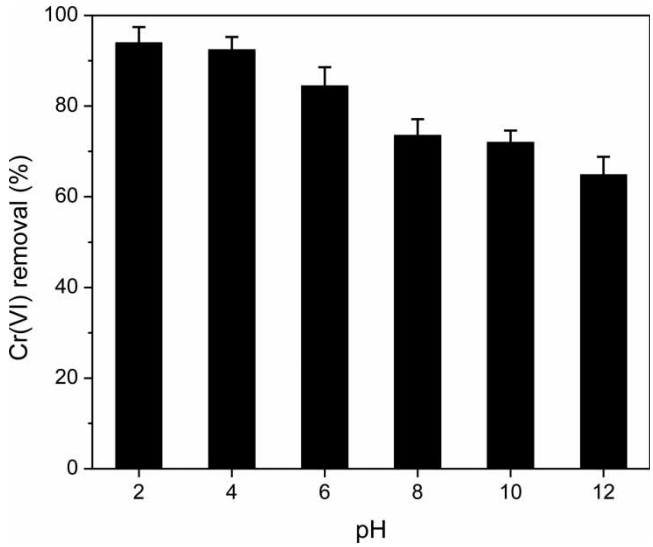

Figure 4 | Effect of initial solution pH on Cr(VI) removal by M-NZVI. The M-NZVI particles have a (MCM-41):Fe^0 mass ratio of 4:1. $[Cr(VI)]_0 = 100$ mg/L, $[M\text{-}NZVI]_0 = 0.5$ g/L, and reaction time = 60 min.

Effect of M-NZVI dosage

Figure 5 shows that increasing the dosage of M-NZVI enhances the Cr(VI) removal efficiency. With M-NZVI dosage increasing from 0.3 to 1.2 g/L, the Cr(VI) removal efficiency increases from 77.2 to 98.3% within 60 min. It is believed that the Cr(VI) reductive reaction occurs on the surfaces of NZVI (Wu *et al.* 2009). As the NZVI mass concentration increases, the reactive iron sites increase proportionally, leading to the increment of Cr(VI) removal efficiency. At higher dosage of M-NZVI (>1.2 g/L), however, the Cr(VI) removal efficiency decreases slightly as the iron dosage increases, which is ascribed to the splitting effect of flux (concentration gradient) and mass transfer barrier between adsorbate and adsorbent (Nandi *et al.* 2009).

Kinetics analysis

In general, Cr(VI) removal by NZVI particles is assumed to be a first-order reaction with respect to Cr(VI) concentration, ignoring NZVI dosage (Alidokht *et al.* 2011; Singh *et al.* 2011). The kinetic expression can be represented in the following equation:

$$C_t = C_0 e^{-kt} \tag{2}$$

where C_0 and C_t are the initial and residual Cr(VI) concentration (mg/L) at time t (min), respectively; k denotes the observed pseudo-first-order rate constant (min^{-1}).

When the reaction occurs in water/NZVI interphase, it is difficult to reach 100% removal efficiency of Cr(VI) due to the limitations in solid–liquid phase-transfer. Thus, Equation (2) is modified as Equation (3) as follows:

$$C_t = C_0 e^{-kt} \times \alpha \tag{3}$$

where α is the variation coefficient to the ideal first-order kinetic (1.0 denotes ideal first-order kinetic, the larger the deviation from 1.0, the less fit the first-order kinetics). After integration and rearranging, with the initial conditions $C_t = C_0$ at $t = 0$, the Equation (3) becomes

$$\ln(C_0/C_t) = kt - \ln\alpha \tag{4}$$

Figure 6 presents the plot for the removal of Cr(VI) by M-NZVI particles using the pseudo-first-order kinetics. As shown, the modified first-order model is good for modeling the kinetics of the whole process. The k value of 0.0168/min and α value of 0.955 are obtained. The first-order rate constant is in the same order of magnitude when compared with the results of Shi *et al.* (2011), who reported a higher observed rate constant of 0.0275/min and a lower rate constant of 0.0083/min in the removal of 50 mg/L Cr(VI) by 3 g/L bentonite-supported NZVI.

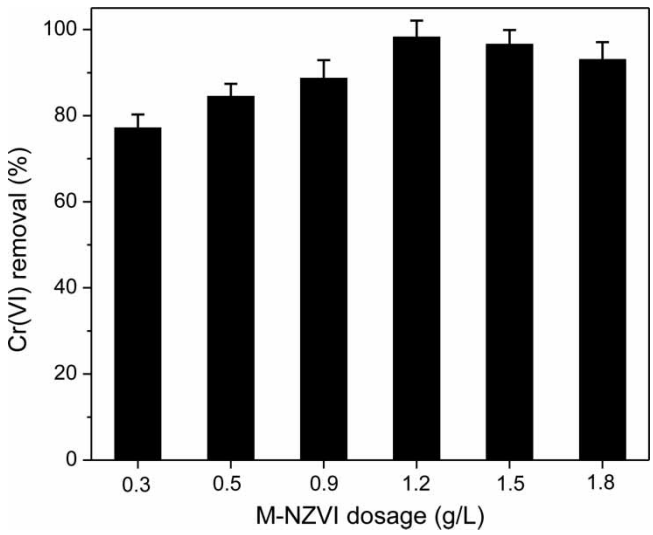

Figure 5 | Effect of M-NZVI dosage on Cr(VI) removal by M-NZVI. The M-NZVI particles have a (MCM-41):Fe^0 mass ratio of 4:1. $[Cr(VI)]_0 = 100$ mg/L, reaction time = 60 min, and $[pH]_0 = 6.0$.

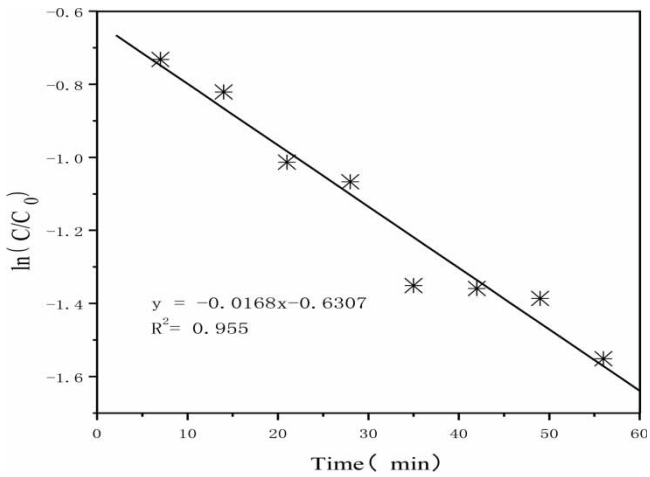

Figure 6 | Pseudo-first-order kinetic model for Cr(VI) removal by M-NZVI. The M-NZVI particles have a (MCM-41):Fe^0 mass ratio of 4:1. $[Cr(VI)]_0 = 100$ mg/L, $[M\text{-}NZVI]_0 = 1.0$ g/L, and $[pH]_0 = 6.0$.

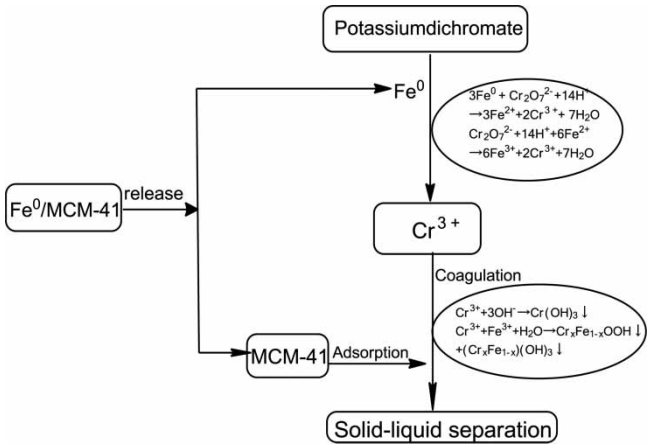

Figure 7 | Proposed mechanism for the reduction of Cr(VI) using M-NZVI.

The removal process of Cr(VI) and the reaction mechanism of M-NZVI are discussed in this study. In the reaction process of Cr(VI) reduction on M-NZVI, M-NZVI particles are evenly dispersed in aqueous solution. After a period of time, the MCM-41 layer of iron surface is completely dissolved in aqueous solution, which exposes Fe^0 to the water. The pathway for removing Cr(VI) in aqueous solution is summarized in Figure 7.

CONCLUSIONS

In this study, ZVI nanoparticles were prepared by using the rheological phase reaction method, employing MCM-41 as a stabilizer. The synthesized M-NZVI particles have higher reactivity and stronger antioxidant activity than bare NZVI due to reduction of aggregation and increased specific surface area. Batch experiments indicate that the Cr(VI) removal increases as the M-NZVI dosage ($\leq$1.2 g/L) increases, and falls as the initial pH increases. The kinetics of Cr(VI) reduction is developed as a modified pseudo-first-order reaction. These results demonstrated that the M-NZVI prepared in this study can be an efficient, effective, and promising remediation material to remove Cr(VI) from wastewater.

ACKNOWLEDGEMENTS

This work has been funded by the National Natural Science Foundation of China (No. 51268018). The authors are grateful to the National Engineering Research Center for Domestic and Building Ceramics (JCU) for assistance in the analytical measurements.

REFERENCES

Alidokht, L., Khataee, A. R., Reyhanitabar, A. & Oustan, S. 2011 Reductive removal of Cr(VI) by starch-stabilized Fe^0 nanoparticles in aqueous solution. *Desalination* **270**, 105–110.

Alowitz, M. J. & Scherer, M. M. 2002 Kinetics of nitrate, nitrite, and Cr(VI) reduction by iron metal. *Environ. Sci. Technol.* **36**, 299–306.

Chrysochoou, M., Ferreira, D. R. & Johnston, C. P. 2010 Calcium polysulfide treatment of Cr(VI)-contaminated soil. *J. Hazard. Mater.* **179**, 650–657.

Cong, C. J., Liao, L., Li, J. C., Fan, L. X. & Zhang, K. L. 2005 Synthesis, structure and ferromagnetic properties of Mn-doped ZnO nanoparticles. *Nanotechnology* **16**, 981–987.

Fang, Z., Qiu, X., Huang, R., Qiu, X. & Li, M. 2011 Removal of chromium in electroplating wastewater by nanoscale zero-valent metal with synergistic effect of reduction and immobilization. *Desalination* **280**, 224–231.

Geng, B., Jin, Z., Li, T. & Qi, X. 2009 Kinetics of hexavalent chromium removal from water by chitosan-Fe^0 nanoparticles. *Chemosphere* **75**, 825–830.

Güell, R., Anticó, E., Salvadó, V. & Fontàs, C. 2008 Efficient hollow fiber supported liquid membrane system for the removal and preconcentration of Cr(VI) at trace levels. *Sep. Purif. Technol.* **62**, 389–393.

Jagupilla, S. C., Moon, D. H., Wazne, M., Christodoulatos, C. & Kim, M. G. 2009 Effects of particle size and acid addition on the remediation of chromite ore processing residue using ferrous sulfate. *J. Hazard. Mater.* **168**, 121–128.

Kima, H. J., Kima, J. M., Kimb, W. S., Kooc, H. J., Baed, D. S. & Kima, H. S. 2011 Synthesis of $LiFePO_4$/C cathode materials through an ultrasonic-assisted rheological phase method. *J. Alloy. Compd.* **509**, 5662–5666.

Kotaś, J. & Stasicka, Z. 2000 Chromium occurrence in the environment and methods of its speciation. *Environ. Pollut.* **107**, 263–283.

Kresge, C. T., Leonowicz, M. E., Roth, W. J., Vartuli, J. C. & Beck, J. S. 1992 Ordered mesoporous molecular sieves synthesized by a liquid-crystal template mechanism. *Nature* **359**, 710–712.

Li, Y., Li, J. & Zhang, Y. 2012 Mechanism insights into enhanced Cr(VI) removal using nanoscale zerovalent iron supported on the pillared bentonite by macroscopic and spectroscopic studies. *J. Hazard. Mater.* **227**, 211–218.

Masood, F. & Malik, A. 2011 Hexavalent chromium reduction by *Bacillus* sp. strain FM1 isolated from heavy-metal contaminated soil. *Bull. Environ. Contam. Toxicol.* **86**, 114–119.

Mielczarski, J. A., Atenas, G. M. & Mielczarski, E. 2005 Role of iron surface oxidation layers in decomposition of azo-dye

water pollutants in weak acidic solutions. *Appl. Catal. B: Environ.* **56**, 289–303.

Nahuel Montesinos, V., Quici, N., Beatriz Halac, E., Leyva, A. G., Custo, G., Bengio, S., Zampieri, G. & Litter, M. I. 2014 Highly efficient removal of Cr(VI) from water with nanoparticulated zerovalent iron: Understanding the Fe(III)–Cr(III) passive outer layer structure. *Chem. Eng. J.* **244**, 569–575.

Nandi, B. K., Goswami, A. & Purkait, M. K. 2009 Adsorption characteristics of brilliant green dye on kaolin. *J. Hazard. Mater.* **161**, 387–395.

Richard, F. C. & Bourg, A. 1991 Aqueous geochemistry of chromium: a review. *Water Res.* **25**, 807–816.

Shi, L. N., Lin, Y. M. & Zhang, X. 2011 Synthesis, characterization and kinetics of bentonite supported nZVI for the removal of Cr(VI) from aqueous solution. *Chem. Eng. J.* **171**, 612–617.

Singh, R., Misra, V. & Singh, R. P. 2011 Synthesis, characterization and role of zero-valent iron nanoparticle in removal of hexavalent chromium from chromium-spiked soil. *J. Nanopart. Res.* **13**, 4063–4073.

Wang, Q., Qian, H., Yang, Y., Zhang, Z., Naman, C. & Xu, X. 2010 Reduction of hexavalent chromium by carboxymethyl cellulose-stabilized zero-valent iron nanoparticles. *J. Contam. Hydrol.* **114**, 35–42.

Wang, Y., Fang, Z., Liang, B. & Tsang, E. P. 2014 Remediation of hexavalent chromium contaminated soil by stabilized nanoscale zero-valent iron prepared from steel pickling waste liquor. *Chem. Eng. J.* **247**, 283–290.

Wu, Y., Zhang, J., Tong, Y. & Xu, X. 2009 Chromium(VI) reduction in aqueous solutions by Fe_3O_4-stabilized Fe^0 nanoparticles. *J. Hazard. Mater.* **172**, 1640–1645.

Yang, G., Deng, Y. & Wang, J. 2014 Non-hydrothermal synthesis and characterization of MCM-41 mesoporous materials from iron ore tailing. *Ceram. Int.* **40**, 7401–7406.

Zazo, J. A., Paull, J. S. & Jaffe, P. R. 2008 Influence of plants on the reduction of hexavalent chromium in wetland sediments. *Environ. Pollut.* **156**, 29–35.

Zhang, P., Jin, C., Zhao, Z. & Tian, G. 2010 2D crossed electric field for electrokinetic remediation of chromium contaminated soil. *J. Hazard. Mater.* **177**, 1126–1133.

First received 25 September 2014; accepted in revised form 26 October 2014. Available online 12 December 2014